IMA Journal of Applied Mathematics (1983) **31**, 13–35

A Stable and Accurate Numerical Method to Calculate the Motion of a Sharp Interface Between Fluids

A. J. ROBERTS

*D.A.M.T.P., Silver St, Cambridge CB3 9EW**

[Received 15 December 1982 and in revised form 21 June 1983]

A spectrally accurate numerical method, which is also simple to implement, is derived to calculate the motion of a fluid interface. A numerical instability, typical of algorithms for this problem, is investigated via a linearizing approximation which shows that a trivial adjustment of the algorithm renders it numerically stable while retaining high accuracy. To test for the correct implementation of the algorithm, non-linear simultaneous equations are formulated using time derivative information only from the coded procedure, whose solutions describe progressive interfacial waves of permanent form. The behaviour of this type of algorithm when variations in the point spacing occurs along the interface is investigated and found to cause "scattering" of travelling wave modes.

1. Introduction

IN MANY SITUATIONS density stratification in the vertical is a dominant feature of fluid motion. Such stratification often comprises a series of jumps in the density across relatively localized regions (in the vertical); an air–water interface is one of the most obvious examples. For many purposes the density jump may be assumed to occur in an infinitesimally thin interface. The time dependent behaviour of such an interface is important as breaking water waves exert extreme forces on marine structures (Brevig, Greenhow & Vinge, 1981; Greenhow, Vinge, Brevig & Taylor, 1982). Here we formulate and solve numerically accurate equations which describe the time evolution of an interface between two fluids of different densities.

Attention is restricted to the horizontally periodic two-dimensional motion of an interface between two inviscid, irrotational, incompressible and infinitely deep fluids. It turns out to be no more computationally expensive to calculate such an interfacial motion than it is to calculate a free-surface fluid motion.

There are a number of physical effects that should be considered before the mathematical model described here is applied. The equations do not describe an interface in which there is a smooth change in the density, where "smooth change" presumably means on a scale larger than the mesh point spacing. Of interest here is a paper by Moore (1978) in which he derives equations governing the behaviour of a vortex sheet of small but finite thickness. Also we have excluded viscosity under the assumption that the time intervals investigated are too small for viscosity to act. However, if capillary waves are generated by interfacial tension then viscosity may

* Present address: Department of Applied Mathematics, University of Adelaide, G.P.O. Box 498, Adelaide, South Australia 5001.

0272-4960/83/040013+23 $03.00/0

be significant (see Ferguson, Saffman & Yuen, 1978); the addition of some representation of viscosity may also be numerically desirable (see Section 6). Nor is the possibility of flow separation at the interface, which may be particularly important in the lighter fluid when the fluids are of very different densities, catered for in the model.

Numerical solutions describing free-surface flows, a special case of a density interface, have been pioneered by Zaroondy & Greenberg (1973) for a solitary wave and by Longuet-Higgins & Cokelet (1976) for periodic waves. Recently Vinje & Brevig (1981) and Baker, Merion & Orszag (1982) have also developed algorithms to calculate free surface flows numerically. Equations governing a sharp interface have been derived by Birkhoff (1962) and used by Pullin (1982) and Baker *et al.* (1980) to investigate some of the instabilities that occur on an interface.

In Section 2 we derive an integral equation approach to the equations describing the evolution of an interface, similar to both Baker *et al.* (1982) and Pullin (1982). The equations derived and their numerical approximations (Section 3) have several advantages over previous algorithms: accuracy, stability and simplicity. In Section 4 a numerical instability which occurs in all other algorithms (a notable exception being the algorithm of Vinje & Brevig, 1981) is analysed in the context of our numerical equations. The analysis indicates that a particular trivial modification to the algorithm is sufficient to make it numerically stable. It should be noted that an alternative mechanism for the generation of a numerical instability has been described by Moore (1982). Either or both of these instabilities may be present depending upon the details of the algorithm used.

To test the derived algorithm (Section 5) we formulate equations which can be used with the algorithm to compute arbitrary progressive interfacial waves of permanent form. These can then be compared with well-known solutions. In Section 6 we investigate the effect of a numerically introduced inhomogeneity and find that travelling waves can be partially reflected, causing serious qualitative errors to occur in some circumstances.

2. Equations of Motion

In this section we derive the equations governing the unsteady motion of a sharp interface between two inviscid and incompressible fluids of different densities when the motion is assumed periodic in the horizontal direction (Fig. 1). Quantities relating solely to the upper or lower fluids are denoted by the subscripts 2 and 1 respectively. The interface is represented parametrically and is a linear-plus-periodic function of the parameter (usually j) with an arbitrary period N. For convenience the explicit dependence of quantities upon the time and the j parameter will usually be omitted. Primes will denote differentiation with respect to the interface parameter, where necessary the explicit dependence upon the interface parameter will be denoted by the subscripts j or k.

The interface parameter j has a dual nature. On the one hand it can vary continuously and parameterizes an exact interface. On the other hand, the period N will be chosen to be integral and the fluid particles on the interface labelled by $j = 1, 2, \ldots, N$ are the basis of the numerical discretization. This duality allows the

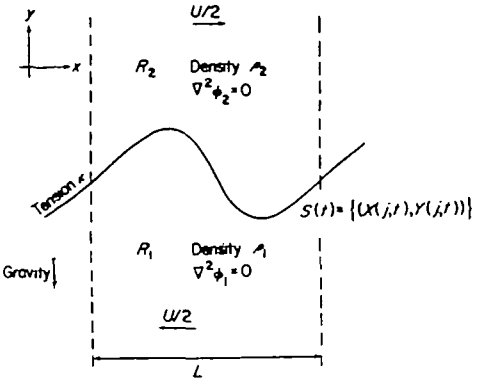

FIG. 1. Sketch of one wavelength of an interface to show the flow geometry and the physical effects considered.

notation to be more compact and permits an easier transformation of the equations between their continuous and discrete forms.

Following Holyer (1979) we non-dimensionalize the problem by scaling quantities with respect to the reference length $L/2\pi$, the reference time $[g(2\pi/L)(\rho_1-\rho_2)/(\rho_1+\rho_2)]^{-1/2}$ and the reference density ρ_1. The scaled density of the lower fluid is thus unity and we let the scaled density of the upper fluid (ρ_2/ρ_1) be denoted by ρ. This scaling ensures a unit wave speed of an infinitesimal wave of wavelength 2π on an interface without shear or tension. The definition of the reference time thus requires the density of the upper fluid to be less than that of the lower fluid and it follows that this scaling cannot be used to study the Rayleigh–Taylor instability.

To follow the motion of the interface we define the differential operator

$$D/Dt = \partial/\partial t + \mathbf{q}_1 . \nabla, \tag{2.1}$$

which gives the derivative following the motion of a particle of the lower fluid on the interface since $\mathbf{q}_l = (u_l, v_l)$ is defined to be the velocity of the lower fluid if $l = 1$, and the upper fluid if $l = 2$. Representing the interface, parametrically in j, by $(X(j, t), Y(j, t))$ the equations that require the interface to follow the motion of particles from the lower fluid at the interface are

$$\partial X/\partial t = Dx/Dt = u_1 \quad \text{and} \quad \partial Y/\partial t = Dy/Dt = v_1 \quad \text{on } S(t). \tag{2.2}$$

In general it is possible to follow hypothetical particles whose velocities are arbitrary linear combinations of the upper and lower fluids velocities at the interface (provided the sum of the weights is precisely unity). However, we do not formulate such a possibility (although the necessary modifications are relatively simple) because we find in Section 4 that the numerical algorithm can be made numerically stable if we follow one fluid or the other, but not in general a combination of both.

The motion in each fluid is assumed irrotational and so the velocities in each fluid can be expressed in terms of a velocity potential, ϕ_1 in the lower fluid and ϕ_2 in the upper fluid. To require that the two fluids do not separate or cross over at the interface we must have

$$\partial\phi_1/\partial n = \partial\phi_2/\partial n \quad \text{on } S(t), \tag{2.3}$$

where n is a co-ordinate measuring distance normal to the interface. The remaining condition at the interface specifies the necessary pressure jump across the interface to be

$$p_2 - p_1 = \kappa/R_s \quad \text{on } S(t), \tag{2.4}$$

where κ is the non-dimensional coefficient of interfacial tension and R_s is the radius of curvature of the interface which is given by

$$1/R_s = (X'Y'' - Y'X'')/(X'^2 + Y'^2)^{3/2}.$$

The pressures p_2 and p_1 are, by Bernoulli's equation,

$$\begin{aligned} p_1 &= -\partial\phi_1/\partial t - [(1+\rho)/(1-\rho)]y - \tfrac{1}{2}\mathbf{q}_1^2 \quad \text{in } R_1, \\ p_2/\rho &= -\partial\phi_2/\partial t - [(1+\rho)/(1-\rho)]y - \tfrac{1}{2}\mathbf{q}_2^2 \quad \text{in } R_2. \end{aligned} \tag{2.5}$$

Define

$$\phi(j, t) = \phi_1 - \rho\phi_2 \quad \text{on } S(t), \tag{2.6}$$

(the periodicity requires that $\phi(j+N, t) - \phi(j, t) = -(1+\rho)\pi U$) then, using Equation (2.5), Equation (2.4) becomes

$$\partial\phi/\partial t = D(\phi_1 - \rho\phi_2)/Dt = -(1+\rho)Y + \tfrac{1}{2}\mathbf{q}_1^2 + \tfrac{1}{2}\rho\mathbf{q}_2^2 - \rho\mathbf{q}_1 \cdot \mathbf{q}_2 + \kappa/R_s. \tag{2.7}$$

Equations (2.2) and (2.7) calculate the time derivative of the quantities $X(j, t)$, $Y(j, t)$ and $\phi(j, t)$ given their values and the velocities of the two fluids at the interface.

The velocities at the interface may be calculated from the knowledge of X, Y and ϕ. We look for ϕ_1 and ϕ_2 to be the real part of a complex potential $f(z)$, $z = x + iy$, for the fluid velocities in the domains R_1 and R_2 respectively. The function $f(z)$ will be defined by a distribution of singularities on the interface $S(t)$, in fact the interface will be a vortex sheet. The connecting Equation (2.3) will thus automatically be satisfied and a net shear across the interface will be provided by requiring some non-zero net amount of vorticity in each wavelength. Hence

$$f(z) = \frac{-i}{2\pi} \int_{-\infty}^{\infty} a_j \log(z - Z_j)\, dj,$$

where a_j is the vorticity strength per unit j and $Z_j = X_j + iY_j$. Using the periodicity, the velocity fields of the fluids can then be written as

$$df/dz = u - iv = \frac{-i}{4\pi} \int_0^N a_j \cot[(z - Z_j)/2]\, dj.$$

As we let z tend to Z_k from the upper or lower fluid we can then calculate the velocities of the two fluids at the interface to be

$$(df/dz)_k = \frac{-i}{4\pi} \int_0^N a_j \cot[(Z_k - Z_j)/2]\, dj \mp \frac{a_k}{2Z_k'}, \tag{2.8}$$

where the upper (lower) alternative gives the upper (lower) fluid's velocity (taking the time derivative of this equation just gives Equation (2) of Baker *et al.*, 1980). The integral is a Cauchy principle value integral and its derivation involves the use of Plemlj formulae. By using the chain rule to calculate df/dj on the interface, the real

part of which gives ϕ'_{2_j} or ϕ'_{1_j}, this last equation gives

$$\phi'_k = \tfrac{1}{2}(1+\rho)a_k + \frac{1-\rho}{4\pi}\int_0^N a_j \,\mathrm{Im}\,\{Z'_k \cot[(Z_k - Z_j)/2]\}\,dj, \tag{2.9}$$

which is an integral equation for the vortex strength a_j given the values of ϕ_j, X_j and Y_j. The far-field boundary condition, $u \to \pm U/2$ as $y \to \pm\infty$, is automatically satisfied as we can see by integrating this equation with respect to k to give

$$\frac{1}{2\pi}\int_0^N a_j\,dj = -U,$$

which ensures that the mean horizontal velocity jump across the interface is just U. From the known vortex strengths the fluid velocities at the interface can be found by evaluating Equation (2.8), the time rate of change of ϕ_j, X_j and Y_j can then be evaluated via Equations (2.2) and (2.7).

It is also useful to calculate some of the various integral invariants of the motion so that the accuracy of the numerical integration can be checked. For most of the integral quantities we adapt the derivations given by Pullin (1982). However, for the kinetic energy density we prefer a formula which only involves quantities that we already know on the interface at any time step (Pullin, 1982, and Baker *et al.*, 1982, use an integral involving the streamfunction at the interface which itself has to be calculated via an integral). The derivation of the formula giving the kinetic energy is described in the Appendix. We find that the difference of the non-dimensional kinetic energy density from that of the undisturbed shear flow can be written as

$$T(t) = \frac{1}{4\pi}\int_0^N [\phi + \tfrac{1}{2}U(1+\rho)X](-Y'u_1 + X'v_1) - \tfrac{1}{2}U[(u_1+\rho u_2)X' + (v_1+\rho v_2)Y' + \tfrac{1}{2}U(1-\rho)X']Y\,dj. \tag{2.10}$$

The difference of the gravitational potential energy density from that of a flat interface is

$$V(t) = \frac{1+\rho}{4\pi}\int_0^N Y_j^2 X'_j\,dj, \tag{2.11}$$

and the average surface energy of the interface relative to that of an undisturbed interface is

$$E_s(t) = \frac{\kappa}{2\pi}\left\{\int_0^N (X_j'^2 + Y_j'^2)^{1/2}\,dj - 2\pi\right\}. \tag{2.12}$$

Conservation of total energy thus requires that

$$E = T(t) + E_s(t) + V(t)$$

is constant.

Also invariant is the average volume flux across the interface

$$\Omega = \frac{1}{2\pi}\int_0^N (v_j X'_j - u_j Y'_j)\,dj, \tag{2.13}$$

which should in fact be zero. The mean vertical position of the interface

$$\bar{Y} = \frac{1}{2\pi}\int_0^N Y_j X_j' \, dj, \tag{2.14}$$

must be invariant as is the difference of the horizontal component of the average momentum from the momentum of the undisturbed shear flow

$$I = \frac{1}{2\pi}\int_0^N \phi_j' Y_j \, dj. \tag{2.15}$$

Because of the presence of gravity neither the vertical momentum nor the angular momentum is conserved.

For later reference we record here the linear solution to the above equations. For a linear wave of wave number m, the position of a particle on the interface at time t whose initial position is parameterized by ξ is

$$X = \xi - (U/2)t - \operatorname{sgn}(m)h \operatorname{Im}\{e^{i(m\xi-\omega t)}\}, \qquad Y = h \operatorname{Re}\{e^{i(m\xi-\omega t)}\}, \tag{2.16}$$

and the combined velocity potential at the particle is

$$\phi = -(1+\rho)[\xi-(U/2)t]U/2 + (h/|m|)\operatorname{Im}\{[(1+\rho)\omega - \rho m U]\, e^{i(m\xi-\omega t)}\}. \tag{2.17}$$

The above form has been chosen so that it is still valid when the frequency is complex, hence these formulae also apply to the initial growth of any naturally occurring unstable modes. The value of the frequency is given by the dispersion relation

$$\omega = mU\rho/(1+\rho) + \{|m|[1+m^2\kappa/(1+\rho)] - m^2U^2\rho/(1+\rho)^2\}^{1/2}, \tag{2.18}$$

The unusual feature to note in this dispersion relation is that the definition of the reference time has caused shear instability (in the absence of interfacial tension) to occur only for values of $U^2 > (1+\rho)^2/(|m|\rho) \geqslant 4/|m|$. Should the reference time be defined to be $(2\pi g/L)^{-1/2}$ (so that, for example, Rayleigh–Taylor instability may be studied) the only changes that need to be made in the governing equations is the replacement of the $(1+\rho)Y$ factor by $(1-\rho)Y$ in Equations (2.5), (2.7) and (2.11).

3. Numerical Approximation

The numerical approximations used to solve the equations derived in the previous section are divided into two parts. They are: the calculation of approximations to the time derivatives of quantities given their values at a set of points on the interface at any time; and the forward integration in time of those quantities. We consider the accurate time integration of a finite set of ordinary differential equations to be a solved problem. Throughout this chapter we integrate in time using the variable-step variable-order Adams method as implemented by the NAG routine DO2CBF. We now describe how accurately and simply to cast the governing equations into the form of a finite set of ordinary differential equations.

Functions are represented by their values at N mesh points which are equispaced on the interval $(0, N]$, that is $j = 1, 2, \ldots, N$. The choice of the exact point on the interface corresponding to each integer value of j is somewhat arbitrary (but see

Section 6). The interface particles that we follow in time are of one fluid or the other (usually the lower fluid).

Accurate differentiation is simply obtained by taking the finite Fourier transform of the function, differentiating this and then inverting to obtain the derivative at the N mesh points. Some of the functions, namely X_j and ϕ_j, are not purely periodic in j but instead have a linear part and a periodic part. Such behaviour can be simply handled once the linear part, which is $2\pi j/N$ for X_j and $-(1+\rho)\pi Uj/N$ for ϕ_j, are known. If N is some power of 2 then this differentiation can be done very economically via the fast Fourier transform algorithm, other values of N cause varying efficiencies. For smooth functions the error in the Fourier differentiation is exponentially small, e^{-bN} say. Stated more generally (and hence more usefully) the error is of a similar order of magnitude as the size of the lowest neglected Fourier component. A comparison between this spectral differentiation and 2nd-, 4th-, 6th- and 8th-order methods is given in Figure 27 of Fornberg & Whitham (1978).

The integrals in Section 2 are all periodic and thus we evaluate them accurately by simply summing the values of the integrand at the mesh points. This procedure also has an error of the same order of magnitude as the largest neglected component in a Fourier decomposition of the integrand.

The kernel of the integral equation (2.9) appears at first sight to be singular for $j = k$. However,

$$\operatorname{Im}\{Z_k' \cot[(Z_k - Z_j)/2]\} \to \operatorname{Im}\{Z_k''/Z_k'\} \quad \text{as } j \to k, \tag{3.1}$$

thus the kernel is not singular and the value of the kernel at $j = k$ is just given by the above limit. The integral equation (2.9) has the useful property that it is diagonally dominant, particularly for small density differences (ρ near 1) and for small wave amplitudes with little shear. This suggests that an iteration procedure may be a more efficient method of solving the discretized integral equation rather than a matrix inversion (Baker *et al.*, 1980, 1982). However, a preliminary test indicates that there is little to be gained unless N is greater than about 32.

The integrand of the principal value integral in Equation (2.8) is singular. The singularity can be removed by subtracting a zero integral whose integrand has exactly the same singularity, thus Equation (2.8) becomes

$$(df/dz)_k = \frac{-i}{4\pi}\int_0^N \left\{a_j \cot[(Z_k - Z_j)/2] - \frac{2\pi}{N}(a_k/Z_k')\cot[\pi(k-j)/N]\right\} dj \mp \frac{a_k}{2Z_k'}. \tag{3.2}$$

The integrand of this integral tends to

$$\frac{Z_k'' a_k}{Z_k'^2} - \frac{2a_k'}{Z_k'} \tag{3.3}$$

as j tends to k. The net contribution of the introduced term in the integral of Equation (3.2) is zero and is only introduced to give a value for the integrand at the singular point $j = k$. Hence the integral in Equation (2.8) is evaluated simply by summing the integrand but using the value (3.3) at the point $j = k$. Equations (3.2) and (3.3) are essentially the same as equations derived by Van der Vooren (1980). To calculate the $O(N^2)$ cotangents needed for the integral it is quicker to calculate the $N \cot(Z_j/2)$s and then calculate $\cot[(Z_k - Z_j)/2]$ via a difference formula for

cotangents. The time derivatives of X, Y and ϕ at the N mesh points are then calculated by evaluating Equations (2.2) and (2.7) at the N mesh points.

This integral equation formulation and discretization is preferred to the conformal mapping technique derived by Fornberg (1980) to calculate a free-surface flow, because the necessary variation of his method to calculate a two-fluid flow would rely heavily on an efficient and accurate interpolation at irregular points: while here the discretization is both simple and accurate, even with relatively few mesh points.

4. Numerical Stability

As first discovered by Longuet-Higgins & Cokelet (1976) an instability develops in the flow, the instability occurring as a sawtooth perturbation to the developing interface profile. The aim of this section is to eliminate this non-physical instability, the simplest case of no interfacial tension is used to facilitate the analysis. and, unless otherwise specified, in this section ρ will be fixed at 0·1.

To study the instability by integrating the ordinary differential equations from various initial profiles is inefficient and often inconclusive (the growth rate of the instability may be undetectable in a trial run of limited duration, or alternatively it may be confused with a real effect). Instead the instability is investigated via an approximation valid for small times or disturbances, we may revert to direct integration to check results; particularly for large wave amplitudes.

The system of ordinary differential equations can be abstractly represented as the non-linear autonomous system

$$d\mathbf{w}/dt = \mathbf{f}(\mathbf{w}), \qquad \mathbf{w}(0) = \mathbf{w}_0 \tag{4.1}$$

which may be linearized to the system

$$d(\mathbf{w}-\mathbf{w}_0)/dt = \mathbf{f}_0 + F(\mathbf{w}-\mathbf{w}_0), \qquad \mathbf{w}(0)-\mathbf{w}_0 = 0. \tag{4.2}$$

Solutions of this equation are approximations to the solutions of Equation (4.1). As the approximation is linear the behaviour of its solutions can be completely understood by considering the eigenvalues and eigenvectors of the array F and the corresponding eigenvector decomposition of $\mathbf{f}_0$. In fact, if λ is an eigenvalue of F, $\mathbf{e}$ the corresponding eigenvector, and f_0, w and w_0 are corresponding coefficients in the eigenvector decomposition of $\mathbf{f}_0$, $\mathbf{w}$ and $\mathbf{w}_0$ respectively, then the approximate solution of Equation (4.1) is

$$\begin{aligned} w - w_0 &= \frac{f_0}{\lambda}\left[e^{\lambda t} - 1\right] + O(\mathbf{f}_0^2 t^3), \quad \lambda \neq 0 \\ &= f_0 t + O(\mathbf{f}_0^2 t^3), \qquad\qquad \lambda = 0. \end{aligned} \tag{4.3}$$

The matrix F also determines the behaviour of small perturbations to the initial state $\mathbf{w} = \mathbf{w}_0$, in particular if $\mathbf{w}_0$ is a stationary point of Equation (4.1), e.g. a flat undisturbed interface, then the eigenvectors of F correspond to the linearized modes and the eigenvalues given the linearized oscillation-frequency/growth-rate about the stationary point. Similarly, if $\mathbf{w}_0$ is not a stationary point of Equation (4.1) then the eigenvalues λ give a quasi-steady oscillation-frequency/growth-rate to those

perturbations of $\mathbf{w}_0$ proportional to the corresponding eigenvector. A similar idea was used by Fornberg & Whitham (1978) to investigate numerically sideband instability in a model non-linear wave equation.

The coefficients of the matrix F are here approximated by simple numerical differentiation giving an error in the coefficients of about 10^{-7}. Isolated eigenvalues and the corresponding eigenvectors are expected to have a similar accuracy, while repeated eigenvalues may have an appropriately larger error.

Because we use Fourier differentiation and integration, the linearized modes on a flat interface are given exactly (see the first column of Table 1), this is true even in the presence of interfacial tension and a net shear. This is a first check on the coding of the procedure to calculate the time derivatives of X, Y and ϕ. It also reassures us that interfacial tension affects the smallest resolved scales in a reasonable manner.

The general pattern of eigenvalues for even N (see the first two columns of Table 1) is that out of the $3N$ eigenvalues there are:

(1) $N-2$ pairs of eigenvalues corresponding to $N-2$ propagating wave modes (without shear the pairs are themselves paired as left- and right-travelling waves having identical frequencies);
(2) N zero eigenvalues corresponding to the N degrees of freedom allowed by the freedom to spread the mesh points (almost) arbitrarily along the interface;
(3) one set of four eigenvalues corresponding to a sawtooth instability, two being growing modes and two decaying, with a height dependent growth rate.

For odd N the pattern is similar but with $N-4$ stable wave modes and with four

TABLE 1

Eigenvalues of the matrix F from the linearization of the set of ordinary differential equations, each eigenvalue listed represents itself and its negative. The value of the parameters used are $N = 16$, $\rho = 0{\cdot}1$, $U = 0$ *and* $\kappa = 0$

Wavenumber m	Unsmoothed $h = 0{\cdot}0$	Unsmoothed $h = 0{\cdot}1$	Five-point smoothed $h = 0{\cdot}0$	Five-point smoothed $h = 0{\cdot}1$
1	*i*1·000000	*i*0·992873	*i*0·999275	*i*0·991273
	*i*1·000000	*i*0·992873	*i*0·999275	*i*0·992966
2	*i*1·414214	*i*1·400956	*i*1·398966	*i*1·383299
	*i*1·414214	*i*1·410810	*i*1·398966	*i*1·396177
3	*i*1·732051	*i*1·716199	*i*1·732051	*i*1·721601
	*i*1·732051	*i*1·726039	*i*1·732051	*i*1·800657
4	*i*2·000000	*i*1·980757	*i*1·647480	*i*1·645283
	*i*2·000000	*i*1·990584	*i*1·647480	*i*1·661425
5	*i*2·236068	*i*2·212877	*i*1·615622	*i*1·572964
	*i*2·236068	*i*2·222657	*i*1·615622	*i*1·609628
6	*i*2·449490	*i*2·423590	*i*1·276197	*i*1·284327
	*i*2·449490	*i*2·433779	*i*1·276197	*i*1·270415
7	*i*2·645751	*i*2·626807	*i*0·722982	*i*0·694148
	*i*2·645751	*i*2·642779	*i*0·722982	*i*0·690406
Sawtooth modes		0·745505		
		0·745505		
Zero eigenvalues	20	16	20	20

(sawtooth) modes which propagate and have non-zero height-dependent real parts (hence two of the modes are unstable).

The presence of the unstable modes in the system confirms that the sawtooth instability is intrinsic to the discretized equations and is not just an instability of the time integration. The unstable modes (for even N) on the wave

$$Z_j = 2\pi j/N + hi\, e^{i2\pi j/N}, \qquad \phi_j = h(1+\rho)\sin(2\pi j/N),$$

are approximately given by the numerically derived empirical formulae

$$\lambda = \pm 0{\cdot}44Nh, \quad Z_j = (-1)^j[iA^* - A\, e^{\pm i2\pi j/N}], \quad \phi_j = 0, \tag{4.4}$$

where * denotes complex conjugation and A is an arbitrary complex number of unit magnitude. The degree of freedom in A is allowed because λ is a repeated eigenvalue. The eigenvalue shows the highly undesirable properties of the instability: the growth rate increases with increasing wave height and also increases with an increasing number of mesh points N. For odd N the behaviour of the real parts of the highest modes' eigenvalues is similar.

This sawtooth instability has been overcome by Longuet-Higgins & Cokelet (1976) who introduced a smoothing technique that eliminates the instability. Their five-point smoothing was applied here to the values of the functions before each time derivative calculation was started; the resultant set of eigenvalues is given in the third and fourth columns of Table 1. The instability is removed. However, the errors in these eigenvalues are quite large, in fact for about half the wave modes the frequencies are hopelessly incorrect (see also Moore, 1981). This smoothing is thus rejected for our purposes as it effectively halves the number of points used to represent the interface, and the wave modes that it does represent are not represented at all accurately, quite contrary to the spirit of this formulation.

To make further progress in eliminating the instability while maintaining accuracy we have to look closer into the governing equations. The eigenvalues of disturbances to a flat interface in the presence of a net shear across the interface shows a sawtooth instability present. Instead of the pair of growing modes (and a corresponding pair of decaying modes) we get only one growing mode (and one corresponding decaying mode) given approximately by the numerically obtained empirical formulae

$$\lambda = \pm 0{\cdot}38UN, \qquad Z_j = (-1)^j\, e^{\pm i0{\cdot}9154}, \qquad \phi_j = 0, \tag{4.5}$$

The instability is thus seen to be a result of the shear at the interface. The involvement of A in the unstable eigenvector given by Equation (4.4) ensures that at a peak or trough the eigenvector looks very much like the eigenvector given in Equation (4.5). Thus the sawtooth instability on a wave is unphysically induced by the local shear at the peaks and troughs of a wave.

We analyse this instability via some elementary analysis, restricting our attention to the simpler case of even N. Consider a flat interface across which there is a net velocity difference of U which has a small sawtooth perturbation, i.e.

$$Z_j = 2\pi j/N + (2\pi/N)A(-1)^j + B, \qquad \phi_j = -(1+\rho)\pi Uj/N + (-1)^j C, \tag{4.6}$$

where A and B are complex functions and C a real function of time that are, at least

initially, small in magnitude. We wish to derive an equation governing the behaviour of A, the complex amplitude of the sawtooth mode. We represent the $(-1)^j$ component of Z_j in the general form

$$(-1)^j = [(1+l)\,e^{i\pi j} + (1-l)\,e^{-i\pi j}]/2 = \cos(\pi j) + il\sin(\pi j), \tag{4.7}$$

where l is left free to be chosen arbitrarily: $l = \pm 1$ means that we represent the interface perturbation by $e^{\pm i\pi j}$, while $l = 0$ represents the perturbation as $\cos(\pi j)$. Here we see the dual nature of j: for integral j the above equation is an identity, but for continuously varying j the right-hand side interpolates a different interface between the known points for different values of l.

For generality we will follow particles on the interface whose velocities are a constant mixture of the two fluids' velocities. Equation (2.2) is thus modified to

$$\begin{aligned} \partial X/\partial t &= [(1+\alpha)u_1 + (1-\alpha)u_2]/2, \\ \partial Y/\partial t &= [(1+\alpha)v_1 + (1-\alpha)v_2]/2, \end{aligned} \tag{4.8}$$

where α is the constant: $+1$ to follow the lower fluid, -1 to follow the upper fluid, and 0 to follow mid-interface particles. Equation (2.7), giving $\partial\phi/\partial t$, is also modified but the equation is insignificant in the following analysis and we need not detail the changes.

Differentiating Equation (4.6) and evaluating for integral j we find

$$\begin{aligned} \phi'_j &= -(1+\rho)\pi U/N, \\ Z'_j &= (2\pi/N)\{1 + i\pi l A(-1)^j\}, \\ Z''_j &= -(2\pi/N)\pi^2 A(-1)^j. \end{aligned} \tag{4.9}$$

For the above interface the integral Equation (2.9) for the vorticity a_j is thus

$$\frac{1+\rho}{2}\,a_k + \frac{1-\rho}{4\pi}\int_0^N a_j\,\mathrm{Im}\,\{Z'_k \cot[(Z_k - Z_j)/2]\}\,dj = -(1+\rho)\pi U/N. \tag{4.10}$$

Observe that the sawtooth component of the velocity potential, represented by C, does not appear in this equation. Thus there can be no feedback from C into the equations for A, the sawtooth particle displacements. Hence the role of a sawtooth component in the potential is purely passive (this is also predicted from the unstable eigenvectors given by Equations (4.4) and (4.5) which have $\phi_j = 0$).

Equation (4.10) may be solved iteratively to give a sufficient approximation for the vorticity a_j. As a first approximation the contribution from the integral is negligible, of $O(A)$, and hence

$$a_k = -(2\pi/N)U + O(A),$$

which just gives the appropriate velocity jump across a flat interface. As a second approximation we use this expression in the integrand of Equation (4.10) and derive that

$$a_k = -(2\pi/N)U + \frac{(1-\rho)U}{(1+\rho)N}\int_0^N \mathrm{Im}\,\{Z'_k \cot[(Z_k - Z_j)/2]\}\,dj + O(A^2).$$

Using simple summation to evaluate the integral we find

$$a_k = -(2\pi/N) + \frac{(1-\rho)U}{(1+\rho)N} \operatorname{Im} \left\{ \frac{Z_k''}{Z_k'} + \sum_{j=1, j\neq k}^{N} \frac{2\pi}{N} [1 + i\pi l A(-1)^k] \times \cot [\pi(k-j)/N + (\pi/N)A((-1)^k - (-1)^j)] \right\} + O(A^2)$$

$$= -(2\pi/N) + \frac{(1-\rho)U}{(1+\rho)N} \operatorname{Im} \left\{ -\pi^2 A(-1)^k - \frac{2\pi}{N} [1 + i\pi l A(-1)^k] \times \sum_{j=1}^{N-1} \cot [\pi j/N - (\pi/N)(-1)^k A(1-(-1)^j)] \right\} + O(A^2).$$

The sum which appears here is the particular example of the sum

$$\sum_{j=1}^{N-1} [1 + p(-1)^j] \cot [\pi j/N + q(1-(-1)^j)] = -\tfrac{1}{2}N^2 q + O(pq, q^3), \tag{4.11}$$

with $p = 0$ and $q = -(\pi/N)(-1)^k A$. The identity in this equation may be readily checked by numerical evaluation. Using this we then simplify the expression for the vorticity to

$$a_k = -(2\pi/N)U \left[1 + \pi \frac{1-\rho}{1+\rho} \operatorname{Im} \{A\}(-1)^k \right] + O(A^2), \tag{4.12}$$

and hence also

$$a_k' = 0.$$

Equation (4.12) shows that only the vertical sawtooth-excursions of the interface particles generate sawtooth vorticity.

The velocities on the interface may now be evaluated via Equation (3.2). Using simple summation to evaluate the integral we find

$$\int_0^N \dots dj = \frac{Z_k'' a_k}{Z_k'^2} - \frac{2a_k'}{Z_k'} + \sum_{j=1, j\neq k}^{N} a_j \cot [(Z_k - Z_j)/2]$$

$$= \pi^2 UA(-1)^k + \frac{2\pi}{N} U \sum_{j=1}^{N-1} \left[1 + \pi \frac{1-\rho}{1+\rho} \operatorname{Im} \{A\}(-1)^j \right] \times \cot \left[\pi j/N - \frac{\pi}{N}(-1)^k A(1-(-1)^j) \right] + O(A^2)$$

$$= 2\pi^2 UA(-1)^k + O(A^2),$$

where we have used Equation (4.11) with $p = \pi[(1-\rho)/(1+\rho)] \operatorname{Im} \{A\}$ and $q = -(\pi/N)(-1)^k A$ to simplify the sum. Substituting this into Equation (3.2) the fluids' velocities at the interface are

$$u_k - iv_k = \pm U/2 + \frac{\pi U}{2} \left[-i(1 \pm l)A \pm \frac{1-\rho}{1+\rho} \operatorname{Im} \{A\} \right] (-1)^k + O(A^2).$$

Thus the time derivatives of the particle positions as given by Equation (4.8) are

$$\partial X_k/\partial t = -\alpha U/2 + \frac{\pi U}{2}\left\{1-\alpha\left[l+\frac{1-\rho}{1+\rho}\right]\right\} \text{Im}\,\{A\}(-1)^k + O(A^2),$$
$$\partial Y_k/\partial t = \frac{\pi U}{2}\{1-\alpha l\}\,\text{Re}\,\{A\}(-1)^k + O(A^2). \tag{4.13}$$

Writing

$$A = \xi(t) + i\eta(t),$$

and separating out the sawtooth components of Equation (4.13) we find that for small ξ and η

$$d\xi/dt = \frac{NU}{4}\left\{1-\alpha\left[l+\frac{1-\rho}{1+\rho}\right]\right\}\eta, \qquad d\eta/dt = \frac{NU}{4}\{1-\alpha l\}\xi. \tag{4.14}$$

This pair of coupled equations describe the linear behaviour of the sawtooth mode on the interface.

The sawtooth mode will grow exponentially like $e^{\lambda t}$ with the growth-rate λ given by

$$\left(\frac{4\lambda}{NU}\right)^2 = \{1-\alpha l\}\left\{1-\alpha\left[l+\frac{1-\rho}{1+\rho}\right]\right\}, \tag{4.15}$$

which with $\alpha = +1$ and $l = -1$ agrees with the numerically obtained Equation (4.5). The sawtooth mode will be unstable if the right-hand side of this equation is positive; stable but unphysically oscillatory if the right-hand side is negative; and neutrally stable if the right-hand side is zero. Thus choosing l to be in the range

$$\frac{1}{\alpha} - \frac{1-\rho}{1+\rho} \leqslant l \leqslant \frac{1}{\alpha}, \tag{4.16}$$

renders the sawtooth mode stable. The simplest choice is $l = +1$ if we follow the lower fluid ($\alpha = +1$) and $l = -1$ if we follow the upper fluid ($\alpha = -1$). Notice that Equation (4.15) shows that there is no choice of l which makes the motion stable if we follow the mid-interface fluid ($\alpha = 0$). Throughout the rest of this paper we follow particles of the lower fluid and treat a $(-1)^j$ component as $e^{+i\pi j}$ (i.e. $l = +1$). Fully time dependent numerical simulations using this procedure confirm the complete lack of the sawtooth instability (see Figs 2 and 4).

The principal result of this section is that the numerical instability is a result of the numerical approximations invoked to calculate finally the velocities on the interface. For even N the instability can be removed just by appropriate treatment of the highest Fourier mode. The subtlety of the required change perhaps explains why Vinge & Brevig (1981) have not encountered any numerical instability using their algorithm.

There is another, and sometimes more useful, way to eliminate the instability, though at a computational cost. The aim is to calculate the sensitive velocity integral more accurately. We interpolate the X, Y and vorticity distribution (using Fourier interpolation) to find their approximate values at more points on the

interface (e.g. at the N points parameterized by half-integral j). Then evaluating the integral in Equation (3.2) using these interpolated values as well as the original values, we find that the instability is effectively removed at a small computational cost.

However, there is no real advantage here because we can already remove the instability. But, if we use Fourier interpolation to calculate more values of the supplied X, Y and ϕ data (say we calculate data for $2N$ points on the interface) and solve the integral Equation (2.9) for the vorticity at all these points and calculate velocities from Equation (3.2) using all these values then we find that this revised procedure significantly improves our description of the evolving interface. For example, when we simulate a breaking free surface wave (Fig. 2) we can calculate the process of breaking significantly further in time (also, the integral invariants are an order of magnitude more constant with this method, see Fig. 3). However, the additional cost is significant as we have to solve the integral equation at (twice as) many more points.

Comparing this revised procedure with the procedure that follows $2N$ particles on the interface (Figs 2 and 3) we observe that there is little advantage in following the extra points in time. This would tend to indicate that the biggest source of error in this formulation lies in the calculation of the velocity fields and not in the representation of the interface. Putting more points on the interface to solve the integrals is just one way of improving the description of the velocity field.

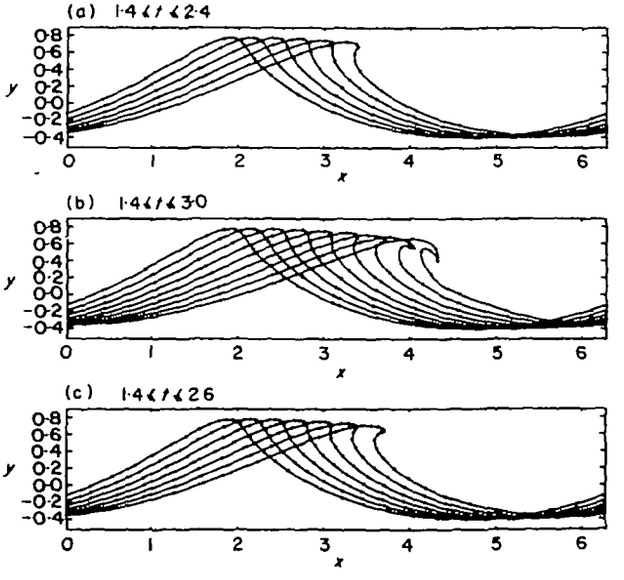

FIG. 2. Three slightly different numerical simulations of the same breaking free-surface gravity wave. The initial profile at time $t = 0$ was $Z_j = \xi + ihe^{i\xi}$, $\phi_j = h \sin \xi$ where $\xi = 2\pi j/N$ and $h = 0{\cdot}5$. The particles followed in time correspond to integral j and are marked by dots; the errors in the profiles are negligible (see Fig. 3). In graph (a) and (b) $N = 16$ points are followed in time, but in (b) the integrals were solved using $N = 32$ points (half of them interpolated) on the interface. In graph (c) $N = 32$ points are followed and used in the integrals.

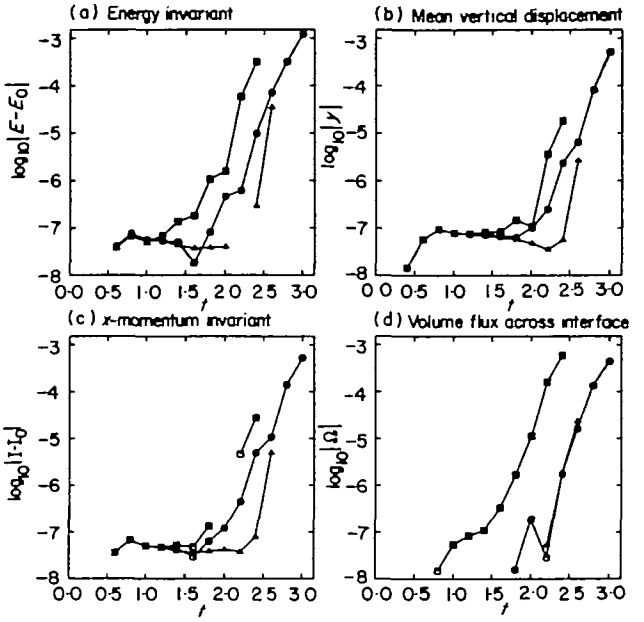

FIG. 3. The behaviour with time of the four integral invariants of the breaking wave motion depicted in Fig. 2. The background error of about 10^{-7} is due to the time-integration tolerance which was set at 10^{-7}. The data come from: □, 2(a) $N = 16$ points; ○, 2(b) $N = 16$ points but 32 points used for the integrals; △, 2(c) $N = 32$ points.

5. Progressive Interfacial Waves of Permanent Form

Having eliminated the instability we now wish to make sure that we have correctly coded the procedure which calculates the time derivatives of X, Y and ϕ given their values at any time. The usual test is to take a well-known progressive wave profile (e.g. a steep free-surface wave) and integrate forward in time for one or more wave periods, checking that the wave profile replicates itself. This was successfully done here using, as an initial profile, an interfacial wave of steepness $h = 0{\cdot}1$ between fluids of density ratio $\rho = 0{\cdot}1$ (Holyer, 1981, private communication).

However, we can carry out another stringent test which has the advantage of checking the procedure over a much wider range of the parameters h, ρ, κ and U. We aim to calculate approximations to the shapes of progressive waves of permanent form using only time-derivative information calculated by our coded procedure for the general unsteady interface motion (unlike Baker *et al.*, 1982, who, to calculate steady interfacial waves, derive an integral equation which is completely separate from their unsteady algorithm). To do this we formulate a set of equations for progressive interfacial waves.

Suppose that the wave travels with a phase speed c, then in a frame of reference moving with the wave the velocity of the particles on the interface must be parallel to the interface,

$$\mathbf{n}.(\mathbf{q}-\mathrm{i}c) = 0 \quad \text{on } S.$$

A vector normal to the interface is $(-Y', X')$ and the velocity $\mathbf{q}$ of the particle that we follow on the interface is given by $(\partial X/\partial t, \partial Y/\partial t)$, hence the above equation becomes

$$-Y'(\partial X/\partial t - c) + X'\,\partial Y/\partial t = 0 \quad \text{on } S. \tag{5.1}$$

In a frame of reference moving with the wave, ϕ_1 and ϕ_2 can only change at a constant rate in time, thus

$$\frac{\partial}{\partial t}(\phi_1 - \rho\phi_2) + c\frac{\partial}{\partial x}(\phi_1 - \rho\phi_2) = \text{const.} \quad \text{on } S.$$

This can be written as

$$\partial\phi/\partial t - (\mathbf{q} - \mathrm{i}c).\nabla(\phi_1 - \rho\phi_2) = \text{const.},$$

where $\mathbf{q}$ is the velocity of the particle which we are following. But from equation (5.1), $\mathbf{q} - \mathrm{i}c$ is parallel to the interface and hence $(\mathbf{q} - \mathrm{i}c).\nabla$ can be written as

$$\frac{(\mathbf{q} - \mathrm{i}c).\mathbf{Z}'}{|\mathbf{Z}'|^2}\,\partial/\partial j.$$

The equation thus becomes

$$\partial\phi/\partial t - \frac{[X'(\partial X/\partial t - c) + Y'\,\partial Y/\partial t]}{X'^2 + Y'^2}\,\phi' = \text{const.} \quad \text{on } S. \tag{5.2}$$

To calculate a wave of steepness h numerically, we assume that the wave is symmetric about the crests and troughs. We then discretize Equations (5.1) and (5.2) by letting the interface be represented by N points, putting $j = 1$ at the wave peak and $j = M + 1$ at the wave trough, where $M = N/2$ and N is even. To fix the wave steepness and the net velocity jump across the interface we put

$$Y_{M+1} = Y_1 - 2h, \qquad \phi_{M+1} = 0, \qquad \phi_1 = \pi(1+\rho)U/2, \tag{5.3}$$

and then symmetry about a wave trough gives

$$Y_{N+1-j} = Y_{j+1}, \qquad \phi_{N+1-j} = -\phi_{j+1}. \tag{5.4}$$

The N unknowns $Y_1, \ldots, Y_M, c, \phi_2, \ldots, \phi_M$ are determined as a solution of N equations: Equation (5.1) at $j = 2, \ldots, M$; Equation (5.2) evaluated at $j = 1, \ldots, M + 1$ (the extra equation is needed to fix the arbitrary constant in the right-hand side); and the side condition

$$\bar{Y} = \frac{1}{2\pi}\sum_{j=1}^{N} Y_j X'_j = 0.$$

This set of non-linear equations can be solved by standard numerical algorithms starting from an initial linear solution or a previously obtained non-linear solution for slightly different values of the parameters. We are free to choose the x-co-ordinates of the particles and for simplicity they were usually chosen to be equispaced in x. Typically $N = 16$ was a sufficient number of points to calculate solutions over most wave heights. For high-gravity waves and for moderately high waves involving interfacial tension or a net velocity jump, more points were needed

to give accurate results (a tuned selection of the x-co-ordinates of the interfacial points may give significant improvements).

Using our general procedure to calculate the time derivatives we find that the solutions of the above equations agreed with known solutions for $\rho = \kappa = 0$ (Cokelet, 1977), $\rho = 0$ and $\kappa \neq 0$ (Hogan, 1980) and $\rho \neq 0$ and $U = \kappa = 0$ (Holyer, 1979). The integral quantities defined in Section 2 also agreed with the known results. As a final check we integrate forward in time from the calculated solutions and confirm that the wave replicates itself after one wave period (Fig. 4). We

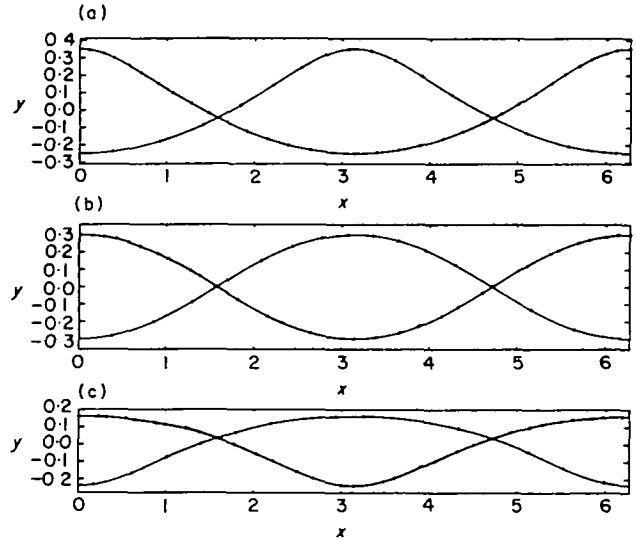

FIG. 4. The propagation of interfacial waves of permanent form: (a) free-surface gravity wave with parameters $h = 0{\cdot}3$ and $\rho = \kappa = U = 0$; (b) Boussinesq interfacial wave, $h = 0{\cdot}3$, $\rho = 1{\cdot}0$, $\kappa = U = 0$; (c) free-surface capillary-gravity wave, $h = 0{\cdot}2$, $\kappa = 1{\cdot}0$, $\rho = U = 0$. Profiles are drawn at times $t = 0$, π/c and $2\pi/c$, where c is the respective wave phase speed.

conclude that our procedure to calculate the time derivatives is correctly coded and can be used to calculate more complicated motions of a sharp interface between two fluids.

Another advantage of this numerical check is that we may immediately calculate properties of some waves that are not well known. Provided a physical solution exists we can calculate approximations to permanent form waves for arbitrary combinations of the parameters h, ρ, κ and U (Saffman & Yuen, 1982, have calculated interfacial waves for some values of h, ρ and U, but they do not include interfacial tension).

6. The Effect of Numerical Inhomogeneity

The equations formulated in Section 2 include a possible interfacial tension. For simple problems which include interfacial tension, numerical algorithms describe the motion to some extent (see Pullin, 1982); but for more complex problems the

algorithm fails [e.g. the generation of capillary waves on the forward surface of a steep free-surface wave is not predicted, instead a "cap" of small-scale structure develops on the crest (Figure 3.7 in Roberts, 1982)]. We suspect that small-scale waves can be trapped in a region in which the followed particles are physically close together relative to other regions of the interface.

This hypothesis is confirmed in this section using the linear analysis of Section 4 applied to a flat undisturbed interface upon which the followed fluid particles are unevenly spread. We set

$$\phi_j = Y_j = 0 \quad \text{and} \quad X_j = 2\pi j/N + a \sin(2\pi j/N), \tag{6.1}$$

where a is a real number, $0 \leqslant a \leqslant 1$, controlling the variation in point spacing. The ratio of distances between the points furthest apart and the points closest together is approximately $(1+a)/(1-a)$. We consider the simplest case of pure-gravity, free-surface waves $\rho = \kappa = U = 0$ (and $N = 16$), the qualitative behaviour of more general parameter values will be similar.

The linearized analysis gives the basic modes of oscillation of the interface, out of which all small-amplitude motions can be synthesized. As a is increased from zero we find that the frequencies of the wave modes shift by an $O(a^2)$ amount and split by an $O(a^4)$ amount (see Fig. 5). The highest wavenumber modes are most affected and the lowest modes least affected (in fact the $m = 1$ mode ($N = 16$) at $a = 0{\cdot}99$ is only changed in the 8th decimal place). Because, at non-zero a, the quadruplets of frequencies split into two pairs the eigenvectors represent standing-wave modes. As in simple quantum-physics problems involving a potential well, travelling-wave modes have to be synthesized by combining adjacent standing wave modes.

Since the highest-wavenumber modes are most affected we plot in Fig. 6 the eigenvectors for the four highest modes ($N = 16$). For $a = 0$ the eigenvectors are

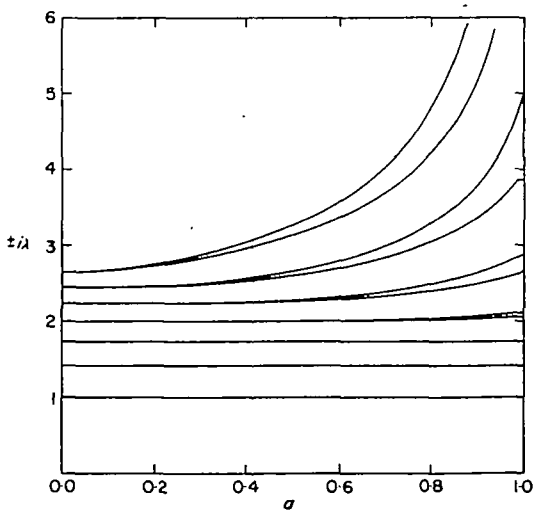

FIG. 5. Frequencies of the basic wave modes on a flat undisturbed interface with an uneven spacing of numerical points; the points are located according to Equation (6.1) with $N = 16$.

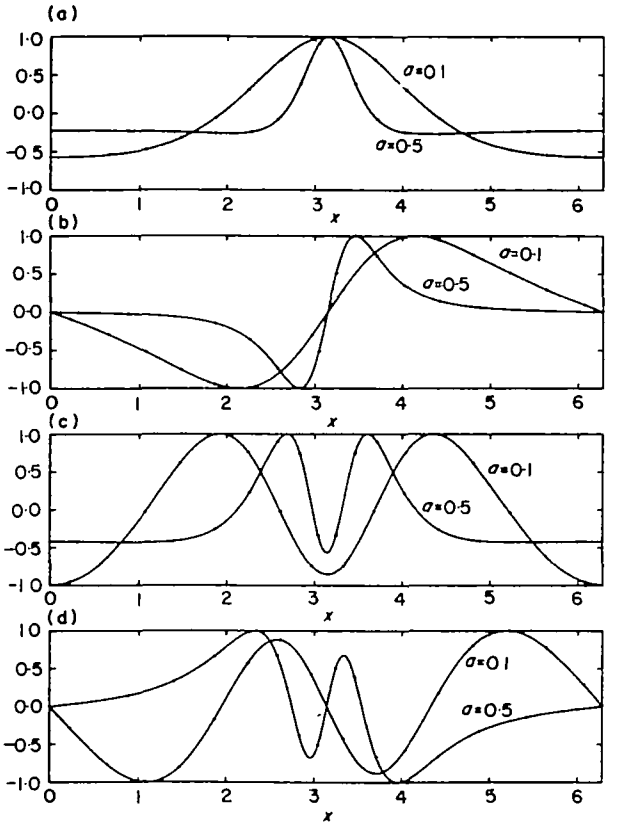

FIG. 6. The four linear wave modes (eigenvectors) of highest frequency on an undisturbed interface with an uneven spacing of points (Equation (6.1) with $N = 16$ and for $a = 0{\cdot}1$ and $a = 0{\cdot}5$). The curves drawn are a smooth interpolation between the points $(-1)^j Y_j$ (indicated by dots) and, in some sense, represent the envelope of these modes. The curves in (a) and (b) are a pair of modes with respective frequencies $\omega = 2{\cdot}6745$ and $2{\cdot}6683$ for $a = 0{\cdot}1$, and $\omega = 3{\cdot}2657$ and $3{\cdot}1344$ for $a = 0{\cdot}5$. The curves in (c) and (d) are a pair of modes with respective frequencies $\omega = 2{\cdot}4507$ and $2{\cdot}4502$ for $a = 0{\cdot}1$, and $\omega = 2{\cdot}6612$ and $2{\cdot}6019$ for $a = 0{\cdot}5$.

purely sinusoidal while for small a the eigenvectors are modified, significantly in the case of the high wavenumber modes, but retain their basic shape.

For moderate a the high-wavenumber modes are largely trapped in regions of small point spacing (the value $a = 0{\cdot}5$ corresponds to a point spacing ratio of 3 which is typical for breaking free-surface waves, see Fig. 2). For half the trapped modes there is a small, but presumably significant, sawtooth component in the region of large point spacing, the other half of the trapped modes are effectively zero there. Thus in this region pairs of nearby modes can only contribute as a standing wave mode. Hence by combining nearby modes we form the picture of a wave which bounces to and fro across the region of small point spacing with a fraction of its energy being radiated at each reflection. For pure-gravity waves a variation in the point spacing need not be as significant as there is a reduced effective gravity at the wave crest where the points are spaced closer together. However, when interfacial

tension is present, capillary-dominated ripples generated at the crest are trapped in a region of small point spacing.

Returning to the low-wavenumber modes, which are barely affected by the variation in point spacing, we observe that the split in the frequencies of a wave mode causes modulations of a travelling wave which occur on a long time scale with a frequency of the order of the frequency difference. Thus variation in point spacing causes quantitative and qualitative errors in a numerical simulation on such long time scales (e.g. eventual complete reflection of a progressive wave).

7. Conclusion

We have considered the evolution of a sharp interface between two fluids of different densities. The approximate equations derived to calculate the motion of the interface numerically are remarkably simple and accurate.

The numerical instability that has plagued previous time-dependent free-surface flow calculations can also occur in this discretization. The normal method of smoothing out this instability, which was introduced by Longuet-Higgins & Cokelet (1976), is unsatisfactory as it is inconsistent with the aim of high accuracy for few mesh points that is aimed for here. By using a linearizing approximation we have found where the instability arises and have slightly altered the algorithm to eliminate the numerical instability. We emphasize that the instability is truly eliminated and not just reduced as Baker *et al.* (1982) have done.

An alternative mechanism for the generation of a sawtooth numerical instability is described by Moore (1982). The mechanism relies upon the numerical dispersion relation of linear waves (the frequency as a function of the wavenumber m for $m = 1, 2, \ldots, N/2$) being of order 1 for the high-wavenumber modes, thus permitting resonance between low wavenumbers and the highest represented wavenumbers. This would commonly occur in algorithms employing finite-difference formulae to calculate spatial derivatives, it does not occur here because spectral differentiation gives the physically correct dispersion relation exactly (except, as we have seen, for the very highest mode $m = N/2$).

There are indications that the primary source of numerical error occurs in the calculation of the velocity fields and not in the representation of the interface (Figs 2 and 3). An algorithm that solves the integral equation using $2N$ interpolated points on the interface improves the description of the velocity fields and hence improves the accuracy of the algorithm (it can also stabilize a previously unstable algorithm).

Finally, we investigated the effect of a numerical inhomogeneity caused by variations in the density of points represented on the interface. It is found that such variations partially reflect travelling wave modes, the highest wavenumber modes being severely affected, causing cumulative errors to build up over time. Such wave scattering should be common to all the similar algorithms devised for this type of problem and indicates that care should be taken in selecting the spacing of numerical points on the interface.

I would like to acknowledge the support of the Association of Commonwealth Universities, the advice of Dr H. E. Huppert who suggested this problem, and the

interest of many others through the course of this research. I also thank my wife for her help with the typing and editing.

References

BAKER, G. R., MERION, D. I. & ORSZAG, S. A. 1980 Vortex simulations of the Rayleigh–Taylor instability. *Phys. Fluids* **23**, 1485–1490.

BAKER, G. R., MERION, D. I. & ORSZAG, S. A. 1982 Generalised vortex methods for free surface flow problems. *J. Fluid Mech.* **123**, 477–501.

BIRKHOFF, G. 1962 *Proc. Sym. Appl. Math. Am. Math. Soc.* **8**, 55–76.

BREVIG, P., GREENHOW, M. & VINGE, T. 1981 Extreme wave forces on submerged cylinders. In *Proc. B.H.R.A. 2nd Int. Symp. on Wave and Tidal Energy*, Cambridge.

COKELET, E. D. 1977 Steep gravity waves in water of arbitrary uniform depth. *Phil. Trans. R. Soc.* **A286**, 183–230.

FERGUSON, W., SAFFMAN, P. & YUEN, H. 1978 A model equation to study the effects of nonlinearity, surface tension and viscosity in water waves. *Stud. appl. Math.* **58**, 165–185.

FORNBERG, B. & WHITHAM, G. B. 1978 A numerical and theoretical study of certain nonlinear wave phenomena. *Phil. Trans. R. Soc.* **A289**, 373–404.

FORNBERG, B. 1980 A numerical method for conformal mappings. *SIAM J. Sci. Statist. Comput.* **1**, 386–400.

GREENHOW, M., VINGE, T., BREVIG, P. & TAYLOR, J. 1982 A theoretical and experimental study of the capsize of Salter's duck in extreme waves. *J. Fluid Mech.* **118**, 221–239.

HOGAN, S. J. 1980 Some effects of surface tension on steep water waves. Part 2. *J. Fluid Mech.* **96**, 417–445.

HOLYER, J. Y. 1979 Large amplitude progressive interfacial waves. *J. Fluid Mech.* **93**, 433–448.

LONGUET-HIGGINS, M. S. & COKELET, E. D. 1976 The deformation of steep surface waves on water. *Proc. R. Soc. Lond.* **A350**, 1–26.

MOORE, D. W. 1978 The motion of a vortex layer of small thickness. *Stud. appl. Math.* **58**, 119–140.

MOORE, D. W. 1981 On the point vortex method. *SIAM J. Sci. Statist. Comput.* **2**, 65–84.

MOORE, D. W. 1982 Resonances introduced by discretisation. *Proc. DFVLR Colloq. on Vortex Motion.*

PULLIN, D. I. 1982 Numerical studies of surface-tension effects in nonlinear Kelvin–Helmholtz and Rayleigh–Taylor instability. *J. Fluid Mech.* **119**, 507–532.

ROBERTS, A. J. 1982 Nonlinear buoyancy effects in fluids. Ph.D. thesis, University of Cambridge.

SAFFMAN, P. G. & YUEN, H. C. 1982 Finite-amplitude interfacial waves in the presence of a current. *J. Fluid Mech.* **123**, 459–476.

VAN DER VOOREN, A. I. 1980 *Proc. R. Soc. Lond.* **A373**, 67.

VINGE, T. & BREVIG, P. 1981 Breaking waves on finite water depths: a numerical study. The Ship Research Institute of Norway, Report R-111.81.

ZAROONDY, S. J. & GREENBERG, M. D. 1973 On a vortex sheet approach to the numerical calculation of water waves. *J. Comput. Phys.* **11**, 440–446.

Appendix: Derivation of a Formula for the Kinetic Energy

We aim to derive a formula giving the kinetic energy in terms of quantities that we have already calculated on the interface at any time step. Consider the periodic slab (bounded by a side C at some x and a side A at $x+2\pi$) shown in Fig. 1 but vertically terminated at large y by a side E at $y=+P$ and by a side B at $y=-P$.

First we calculate an expression for the kinetic energy in the lower fluid and for clarity we omit the subscript 1. Consider the integral

$$T = \frac{\rho}{2} \int_R \nabla . [(\phi - Ux)\nabla(\phi + Ux)]\, dR. \tag{A.1}$$

On one hand we can expand the integrand and show

$$T = \int_R \frac{\rho}{2} (\nabla\phi)^2 - \frac{\rho}{2} U^2\, dR. \tag{A.2}$$

T clearly measures the difference between the kinetic energy in the periodic slab due to the wave motion and the kinetic energy in the slab when there is an undisturbed interface between uniform streams. This quantity can be used in a formula to calculate an energy which we assume is conserved.

On the other hand we can use the divergence theorem to write the integral in Equation (A.1) as an integral over the boundary of the region R,

$$T = \frac{\rho}{2} \int_{\partial R} (\phi - Ux)\partial(\phi + Ux)/\partial n\, ds, \tag{A.3}$$

where the normal $\mathbf{n}$ points out of the region. Separate this into the integral on the interface plus the integrals around the box and, observing that the velocity field is strictly periodic in x, we can write

$$T = \frac{\rho}{2} \int_S \ldots ds + \frac{\rho}{2} \int_A [(\phi_A - \phi_C) - U(x_A - x_C)](u_A + U)\, dy - \frac{\rho}{2} \int_B (\phi - Ux)v\, dx.$$

The second integral is zero because ϕ is a linear-plus-periodic function and the linear part is just Ux. Since the velocity perturbations become very small away from the interface the third integral tends quickly to zero as P (the vertical extent of the box) becomes large.

Writing subscripts in the formulae, the kinetic energy change in the lower fluid due to the motion is thus

$$T_1 = \frac{\rho_1}{2} \int_S (\phi_1 - U_1 x)\partial(\phi_1 + U_1 x)/\partial n\, ds.$$

By exactly similar arguments we find that in the upper fluid

$$T_2 = -\frac{\rho_2}{2} \int_S (\phi_2 - U_2 x)\partial(\phi_2 + U_2 x)/\partial n\, ds.$$

Thus the total kinetic energy change due to the interface motion can be written as

$$T = \frac{1}{2} \int_S [(\rho_1\phi_1 - \rho_2\phi_2) - (\rho_1 U_1 - \rho_2 U_2)x]\, \partial\phi_1/\partial n + [(\rho_1 U_1\phi_1 - \rho_2 U_2\phi_2) - (\rho_1 U_1^2 - \rho_2 U_2^2)x]\, \partial x/\partial n\, ds,$$

where we have used Equation (2.3). But $\partial x/\partial n = -\partial y/\partial s$ and so the last term in the

integrand can be integrated by parts to give

$$T = \frac{1}{2}\int_S [(\rho_1\phi_1 - \rho_2\phi_2) - (\rho_1 U_1 - \rho_2 U_2)x]\,\partial\phi_1/\partial n + [(\rho_1 U_1\,\partial\phi_1/\partial s - \rho_2 U_2\,\partial\phi_2/\partial s) - (\rho_1 U_1^2 - \rho_2 U_2^2)\,\partial x/\partial s]y\,ds. \quad \text{(A.4)}$$

For our purposes we want to calculate the kinetic energy per unit length in the x-direction and so we need to divide this formula by 2π. Also, we write the equation in the dimensionless quantities $\rho_1 = 1$, $\rho_2 = \rho$, $U_1 = -U/2$, $U_2 = U/2$ and $\phi = \phi_1 - \rho\phi_2$. Finally we recognize that

$$\partial[\,]/\partial s\,ds = (X', Y').\nabla[\,]\,dj, \qquad \partial[\,]/\partial n\,ds = (-Y', X').\nabla[\,]\,dj,$$

and so Equation (A.4) can immediately be written as Equation (2.10).